Journal of Power Sources 196 (2011) 8160–8165

Contents lists available at ScienceDirect

Journal of Power Sources

journal homepage: www.elsevier.com/locate/jpowsour

Synthesis of hydrothermally reduced graphene/MnO_2 composites and their electrochemical properties as supercapacitors

Zhangpeng Li[a,b], Jinqing Wang[a,*], Sheng Liu[a,b], Xiaohong Liu[a], Shengrong Yang[a,*]

[a] State Key Laboratory of Solid Lubrication, Lanzhou Institute of Chemical Physics, Chinese Academy of Sciences, Lanzhou 730000, PR China
[b] Graduate University of Chinese Academy of Sciences, Beijing 100080, PR China

ARTICLE INFO

Article history:
Received 21 January 2011
Received in revised form 12 April 2011
Accepted 16 May 2011
Available online 27 May 2011

Keywords:
Graphene
MnO_2
Composite
Supercapacitor

ABSTRACT

Hydrothermally reduced graphene/MnO_2 (HRG/MnO_2) composites were synthesized by dipping HRG into the mixed aqueous solution of 0.1 M $KMnO_4$ and 0.1 M K_2SO_4 for different periods of time at room temperature. The morphology and microstructure of the as-prepared composites were characterized by field-emission scanning electron microscopy, X-ray diffraction, Raman microscope, and X-ray photoelectron spectroscopy. The characterizations indicate that MnO_2 successfully deposited on HRG surfaces and the morphology of the HRG/MnO_2 shows a three-dimensional porous structure with MnO_2 homogenously distributing on the HRG surfaces. Capacitive properties of the synthesized composite electrodes were studied using cyclic voltammetry and electrochemical impedance spectroscopy in a three-electrode experimental setup using 1 M Na_2SO_4 aqueous solution as electrolyte. The main results of electrochemical tests are drawn as follows: the specific capacitance value of HRG/MnO_2–200 (HRG dipped into the mixed solution of 0.1 M $KMnO_4$ and 0.1 M K_2SO_4 for 200 min) electrode reached 211.5 F g^{-1} at a potential scan rate of 2 mV s^{-1}; moreover, this electrode shows a good cyclic stability and capacity retention. It is anticipated that the synthesized HRG/MnO_2 composites will find promising applications in supercapacitors and other devices in virtue of their outstanding characters of good cycle stability, low cost and environmentally benign nature.

1. Introduction

Supercapacitors, one of the most promising electrochemical energy storage systems, have attracted much attention due to their high energy density and long cycle stability [1–3]. Generally, it can be classified into two categories on the basis of the energy storage mechanism, i.e., electric double layer capacitors (EDLCs) and pseudocapacitors [4]. The typical electrode materials of EDLCs are carbon materials with high surface area, which are convenient to store energy in the double layer formed on the surface of carbon materials. While, in the case of the pseudocapacitors, the most used electrode materials are conducting polymers and metal oxides, which transfer the faradic charges between electrolyte and electrode [4].

As a newly found carbon material, graphene has become one of the most studied objectives by material scientists in recent years since Geim and Novoselov succeeded in isolating it from graphite crystals as an individual two-dimensional object [5]. Thanks to its unique physical, chemical, electrical, and mechanical properties, this new material has shown promising prospects for several advanced technological applications, including graphene-based composites, Li-ion batteries, fuel cells, chemical detectors, solar cells, and supercapacitors [6–12]. Recently, the application of graphene in supercapacitors has been attempted by some researchers. For instance, Stoller et al. [13], Vivekchand et al. [14], and Wang et al. [15] reported that the supercapacitor devices based on graphene materials exhibit good electrochemical performance. However, the actual capacitive behavior of pure graphene is much lower than the anticipated value due to the fact that it usually suffers from serious agglomeration during preparation. To boost the electrochemical performance of graphene based supercapacitors remains a great challenge. On the other hand, it has been found that carbon materials combine with pseudocapacitive electrode materials, such as polyaniline (PANI), polyprrole (PPy), RuO_2, IrO_2, and MnO_2, etc., can improve the capacitance of carbon-based supercapacitors [16–18]. Recently, graphene based composites with pseudocapacitive materials have been investigated widely, such as graphene-PANI [19–29], graphene-PPy [30–32], graphene-RuO_2 [33], graphene-MnO_2 [34–37] and other graphene-metal oxide/hydroxide composites [38–44]. Among these pseudocapacitive materials, manganese oxide materials, especially MnO_2, are very attractive because of their distinctive structures and physicochemical properties as well as environmental compatibility and low cost [45]. However, the poor electrical conductivity and

* Corresponding authors. Tel.: +86 931 4968076; fax: +86 931 8277088.
E-mail addresses: jqwang@licp.cas.cn (J. Wang), sryang@licp.cas.cn (S. Yang).

0378-7753/$ – see front matter © 2011 Elsevier B.V. All rights reserved.
doi:10.1016/j.jpowsour.2011.05.036

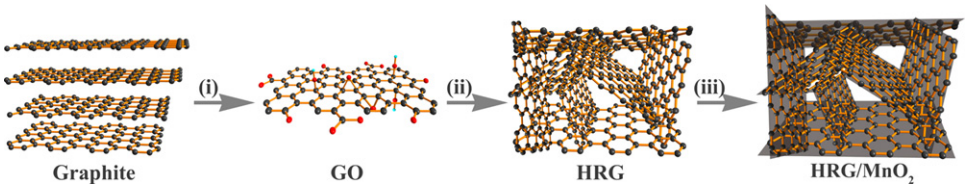

Scheme 1. Illustrations for the formation process of HRG/MnO_2 composite.

densely packed structure limit its deep application in developing high-performance supercapacitors. Considering for the prominent electronic conductivity of graphene and the high capacitance of MnO_2, the combination of graphene with MnO_2 should exhibit the improved electrochemical performance.

Although some works about graphene-MnO_2 composites have been reported [34–37], the investigation of such composite with much simple synthesis method is still an interesting topic. Here, we present a simple approach to prepare hydrothermally reduced graphene/MnO_2 (HRG/MnO_2) composites, which were synthesized by dipping HRG into the mixed solution of 0.1 M $KMnO_4$ and 0.1 M K_2SO_4 for different periods of time. The morphology, microstructure and electrochemical performances of the as-prepared composites were investigated in detail.

2. Experimental

Graphene oxide (GO) was synthesized from graphite powder by a modified Hummers method and our previous work [46,47]. In a typical synthesis, graphite powder was first treated at 1050 °C in air for 15 s. And then, thermally treated graphite powder (1 g) was added to 98% H_2SO_4 (23 mL) in an ice bath. $KMnO_4$ (3 g) was added gradually under stirring and the temperature of the mixture was kept to be below 20 °C. The above mixture was kept at 35 °C for 30 min. Then, deionized water (46 mL) was gradually added keeping the reaction in an ice bath. After 15 min, the mixture was further treated with deionized water (140 mL) and 30% H_2O_2 solution (12.5 mL). The GO was firstly washed with 5% HCl solution, and then dialyzed at 60 °C with stirring until SO_4^{2-} anions could not be detected. The GO slurry was dried in a vacuum oven at 60 °C.

The hydrothermally reduced graphene (HRG) was prepared by a modified method reported by Shi and co-workers [48]. In a typical synthesis, 75 mg GO solid was dispersed in 40 mL water with the aid of ultrasonication. Then, the homogeneous dispersion was sealed in a 50 mL Teflon-lined autoclave and maintained at 180 °C for 12 h. The obtained black solid was filtrated out and dried in a freeze-drying setup. The detailed structural analysis of the as-prepared GO and HRG are provided in Figs. S1 and S2 in Supporting Information section.

To prepare HRG/MnO_2 composites, a certain amount of HRG was dipped into the mixed solution of 0.1 M $KMnO_4$ and 0.1 M K_2SO_4 for 10 and 200 min, respectively. Then the solids were filtered out and dried in vacuum at 60 °C over night. The samples were denoted as HRG/MnO_2–10 and HRG/MnO_2–200 based on the different reaction time. The mass ratios of MnO_2 in the composites were calculated from the weight difference before and after dipping in the mixed solution. The calculated mass ratio of MnO_2 in HRG/MnO_2–10 and HRG/MnO_2–200 were about 25% and 71%, respectively.

The morphology and microstructure of the as-prepared samples were characterized by field-emission scanning electron microscopy (FESEM, JEOL JSM-6701F), atomic force microscopy (AFM, VEECO Nanoscope IIIa), X-ray diffraction (XRD, Rigaku D/Max-2400 diffractometer using Cu Kα radiation and graphite monochrometer, λ = 1.54056 Å), Fourier transformation infrared spectra (FTIR, Bruker IFS66V FTIR spectrometer), Raman microscope (Renishaw inVia Raman microscope with 633 nm line of an Ar ion laser as an excitation source), and X-ray photoelectron spectroscopy (XPS, PHI-5702, Physical Electronics, USA, using a monochromated Al Kα irradiation. The chamber pressure was about 3×10^{-8} Torr under testing condition. Peak deconvolution of C 1s and Mn 3s was accomplished using Origin 7.0).

The electrochemical measurements were performed in a three-electrode cell system with 1 M Na_2SO_4 aqueous solution as electrolyte. The working electrodes were fabricated by mixing the electroactive materials and poly(tetrafluoroethylene) in a mass ratio of 95:5 and dispersed in ethanol to produce homogeneous slurry. The resulting slurry was coated onto the nickel foam current collector (1 cm × 1 cm) using a blade. And then, the electrodes dried at 80 °C for 12 h. The loading mass of each electrode was about 3 mg. Platinum wire and Ag/AgCl (KCl-saturated) electrode were used as counter electrode and reference electrode, respectively. Cyclic voltammetry (CV) and electrochemical impedance spectroscopy (EIS) measurements were performed with a CHI 660C electrochemical workstation. EIS was recorded under the following conditions: AC voltage amplitude of 5 mV, frequency range of 10^5 to 0.1 Hz, and open circuit potential.

3. Results and discussion

As shown in Scheme 1, the formation procedures of HRG/MnO_2 composites are mainly composed of the following three steps, i.e., (i) synthesis of GO from graphite; (ii) preparation of HRG using hydrothermal method followed by a freeze-drying process; (iii) redox deposition of MnO_2 particles onto HRG surfaces in the mixed solution of 0.1 M $KMnO_4$ and 0.1 M K_2SO_4 at room temperature. The proposed depositing mechanism of MnO_2 onto HRG can be illustrated by the following reaction [49,50]:

$$4MnO_4^- + 3C + H_2O \rightleftharpoons 4MnO_2 + CO_3^{2-} + 2HCO_3^- \quad (1)$$

Fig. 1a shows the AFM morphological image and the corresponding cross-section analysis of GO on the silicon substrate. It can be seen that the GO sheets show an average thickness of approximately 0.85 nm, which is in agreement with the reported value of this parameter in the literature [44], indicating that a single-layer GO sheet has been obtained. Fig. 1b–e gives the FESEM images and the corresponding EDS patterns of the as-prepared samples of HRG and HRG/MnO_2–200. It is obvious that the HRG exhibits a 3D porous structure (Fig. 1b). The corresponding EDS spectrum of the HRG indicates that the HRG is only composed of two elements, namely, C and O, as clearly shown in Fig. 1d. After room temperature deposition of MnO_2 for 200 min, the porous structure of the sample is still retained (Fig. 1c). The EDS pattern of HRG/MnO_2–200 shown in Fig. 1e confirms that the existence of the elements of Mn and K besides C and O, which is different from the EDS pattern of HRG, demonstrating the successful deposition of MnO_2. The appearance of K Kα peaks in the sample suggests K^+ co-existing in the MnO_2 matrix arising from the precursors, which always happens during the synthesis process of MnO_2 [51,52].

Fig. 2 shows the XRD patterns of GO, HRG, HRG/MnO_2–10 and HRG/MnO_2–200 samples. XRD pattern of GO reveals an intense and sharp peak located at $2\theta = 11.7°$, corresponding to the characteristic diffraction peak of GO powder. After the hydrothermal processing,

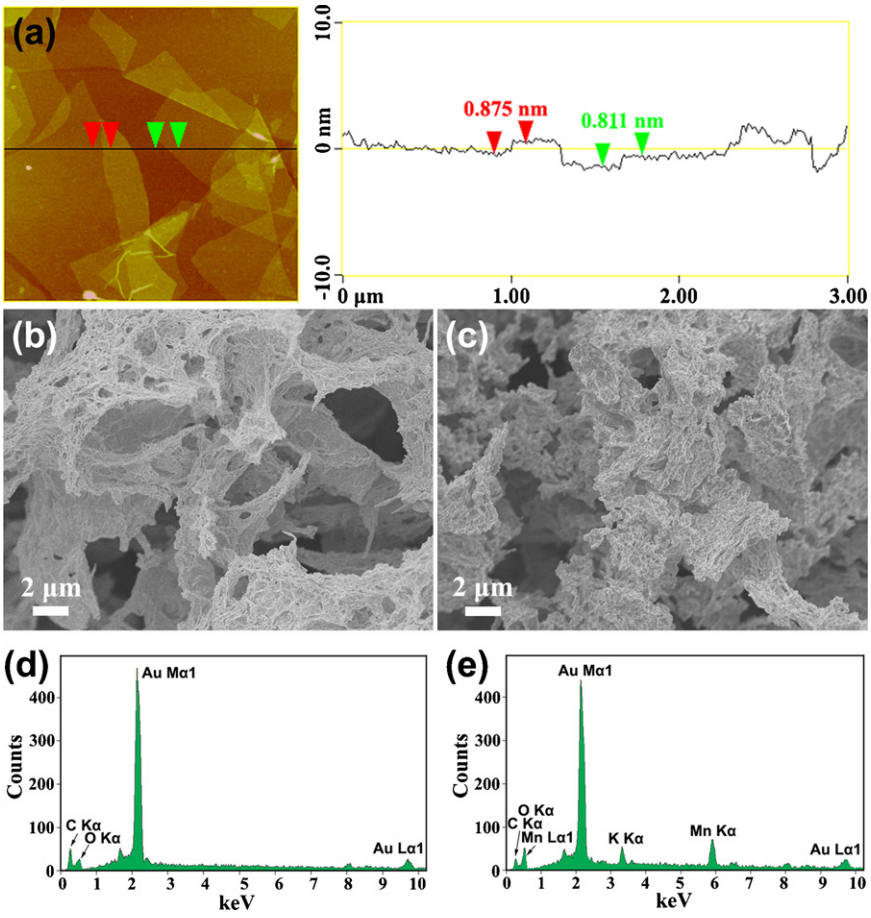

Fig. 1. (a) AFM morphological image and corresponding cross-section analysis of GO; (b and c) FESEM images and (d and e) corresponding EDS patterns of HRG and HRG/MnO_2–200.

the sharp peak at 11.7° disappears and a new broad diffraction peak at $2\theta = 23.4°$ appears in the XRD pattern of HRG, confirming the successful conversion of GO to graphene [53]. In addition, the broad peak profile of HRG slightly lower than the peak of raw graphite ($2\theta = 26.5°$, Fig. S3 in Supporting Information), indicating the destruction of the regular stacking of the graphene sheets in HRG [48,54]. For HRG/MnO_2–10 and HRG/MnO_2–200 samples, the XRD patterns show two new broad diffraction peaks at $2\theta = 37.5°$ (2 1 1) and 49.9° (4 1 1) indexed to MnO_2 (JCPDS No. 44-0141). The broad nature and low relative intensity of the peak profiles suggest amorphous nature of MnO_2 phase in both samples and the very small size of MnO_2 particles.

Raman spectroscopy has been used to investigate the vibrational properties of the as-prepared samples. Fig. 3 gives the Raman spectra of HRG, HRG/MnO_2–10 and HRG/MnO_2–200. The G band around 1590 cm^{-1} and the D band around 1325 cm^{-1} are observed in the Raman spectrum of the HRG, corresponding to the E_{2g} phonon of sp^2-bonded carbon atoms in a two-dimensional hexagonal lattice, as well as the defects and disorder carbon in the graphite layers,

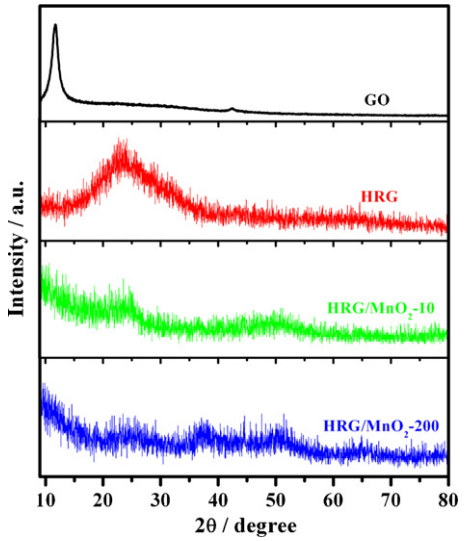

Fig. 2. XRD patterns of GO, HRG, HRG/MnO_2–10 and HRG/MnO_2–200.

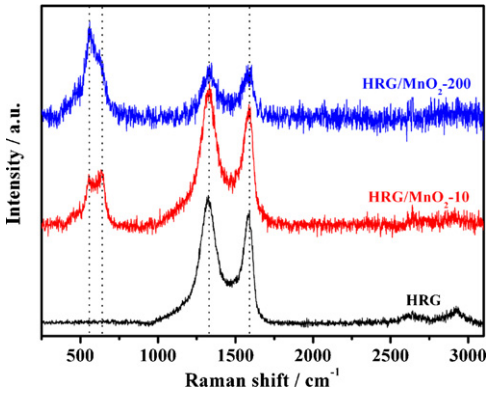

Fig. 3. Raman spectra of HRG, HRG/MnO_2–10 and HRG/MnO_2–200.

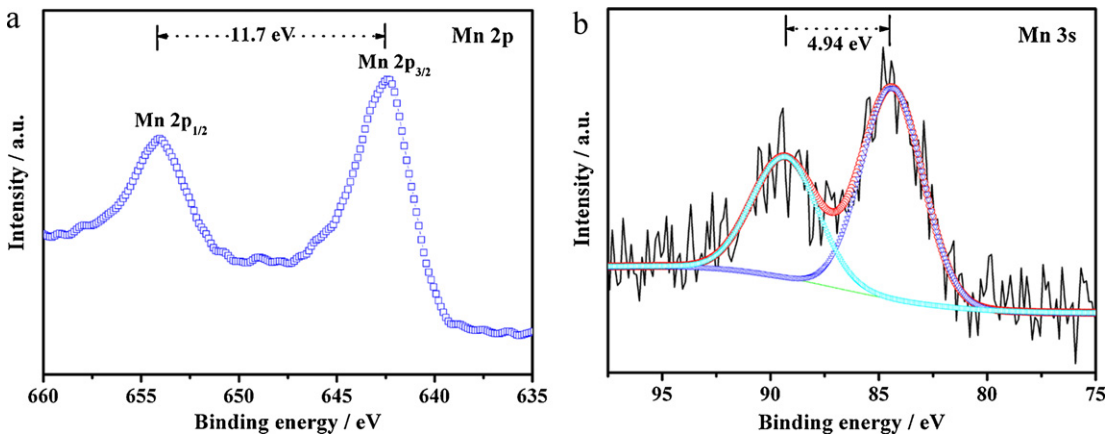

Fig. 4. (a) Mn 2p and (b) Mn 3s XPS spectra of HRG/MnO_2–200.

respectively. As for the Raman spectrum of the HRG/MnO_2–10, two new distinct peaks located at 553 and 633 cm^{-1} appeared, which can be attributed to the Mn–O stretching vibration in the basal plane of MnO_6 and the symmetric stretching vibration (Mn–O) of the MnO_6 group, respectively [55,56]. Similarly, the peak located at 559 cm^{-1} was also observed in the spectrum of HRG/MnO_2–200. These results suggest the integration of MnO_2 and HRG. On the other hand, the intensity ratio of the D to G bond (I_D/I_G) is generally accepted that the I_D/I_G reflects the defect density of carbonaceous materials. For HRG, the I_D/I_G value was calculated as 1.14. Compared with HRG, the I_D/I_G values of HRG/MnO_2–10 and HRG/MnO_2–200 decreased to 1.10 and 1.01 (Table 1), indicating the obvious defect decrease after deposition of MnO_2 particles onto HRG surfaces.

XPS was used to provide further evidence for the successful deposition of MnO_2 on HRG surfaces and to examine the valent state of MnO_2 in HRG/MnO_2. Fig. 4a shows the Mn 2p spectrum of HRG/MnO_2–200, in which the peaks of Mn $2p_{3/2}$ and Mn $2p_{1/2}$ are located at 642.4 eV and 654.1 eV, respectively, with a energy separation of 11.7 eV, are in good agreement with the reported data of Mn $2p_{3/2}$ and Mn $2p_{1/2}$ in MnO_2 [57], indicating the successful deposition of MnO_2 on the HRG surfaces. Additionally, it is well known that the energy separation between the two peaks of Mn 3s doublet (ΔE_b) can be used as an indicator of Mn oxidation state in manganese oxides. A lower valence of Mn leads to a wider splitting of the Mn 3s peaks. As reported by Chigane et al., the ΔE_b of Mn^{3+} and Mn^{4+} oxides are 5.41 and 4.78 eV, respectively [58]. From Fig. 4b, it is found that the ΔE_b of the as-deposited MnO_2 in HRG/MnO_2–200 is 4.94 eV, representing a coexistence of trivalence and tetravalence.

Both CV and EIS measurements were generally applied to evaluate the electrochemical properties of the as-prepared electrode samples. Fig. 5a shows the CV curves of HRG, HRG/MnO_2–10 and HRG/MnO_2–200 electrodes at a scan rate of 40 mV s^{-1} in 1 M Na_2SO_4 electrolyte. It is clear that all of the CV curves for HRG electrode are almost ideally rectangular, exhibiting the typical electrochemical double-layer capacitive behavior with a very rapid current response on voltage reversal at each end potential and high reversibility [35]. Obviously, HRG/MnO_2–10 and HRG/MnO_2–200 electrodes show higher integrated area than HRG electrode, which indicates that the excellent electrochemical performance. The specific capacitances (C_s) were calculated from the CV curves according to the following equation:

$$C_s = \frac{\int I\,dV}{\nu \Delta V m} \quad (2)$$

where I (A) is the response current, ν (V s^{-1}) is the potential scan rate, ΔV (V) is the potential window, and m (g) is the mass of active electrode material. The calculated C_s values of HRG, HRG/MnO_2–10 and HRG/MnO_2–200 electrodes at 40 mV s^{-1} are 74.5, 102 and 135.5 F g^{-1}. In comparison with HRG, the improved electrochemical performance of HRG/MnO_2–10 and HRG/MnO_2–200 electrodes is mainly attributed to the pseudocapacitance of MnO_2 phase and partially from intrinsic electrical double layer capacitance of HRG. Therefore, it is reasonable to believe that the capacitance behavior of HRG/MnO_2–200 electrodes is much better than that of HRG/MnO_2–10 due to the fact that higher MnO_2 loading brings more pseudocapacitive contribution.

EIS measurements were performed in order to further evaluate the electrochemical properties of HRG, HRG/MnO_2–10 and HRG/MnO_2–200 electrodes. Typical Nyquist plots of EIS for these electrodes are displayed in Fig. 5b. All the impedance plots are composed of a semicircle in the high frequency range and a straight line (almost vertical) in the low frequency range. The intersection of the semicircle on the real axis at high-frequency represents the equivalent series resistance (R_s) of the electrode, while the diameter of the semicircle corresponds to the charge-transfer resistance (R_{ct}) of the electrodes and electrolyte interface [31]. Comparing the impedance plots of these electrodes, it is apparent that the values of R_{ct} gradually increase with increasing MnO_2 loading. This result is partially caused by the low conductivity of the HRG/MnO_2 materials after deposition of MnO_2. The straight line in the low frequency range is related to the diffusive resistance of the electrolyte into the interior of the electrode and ion diffusion into the electrode. The almost vertical shape, representing the swift ion diffusion in electrolyte and the adsorption onto the electrode surface, suggests the ideally capacitive behavior of the electrodes.

To get more information on capacitive performance of the as-prepared composites, HRG/MnO_2–200 electrode was selected for the detailed measurements. Fig. 5c displays the CV curves of this electrode at different scan rates of 5, 20, 40, and 60 mV s^{-1} in 1 M Na_2SO_4 electrolyte. All the CV curves are close to a rectangular shape with high symmetry feature, indicating ideal capacitive

Table 1
Raman spectra data of HRG, HRG/MnO_2–10 and HRG/MnO_2–200.

	Mn–O (cm^{-1})	D (cm^{-1})	G (cm^{-1})	I_D/I_G
HRG	–	1325	1590	1.14
HRG/MnO_2–10	553/633	1332	1587	1.10
HRG/MnO_2–200	559	1344	1582	1.01

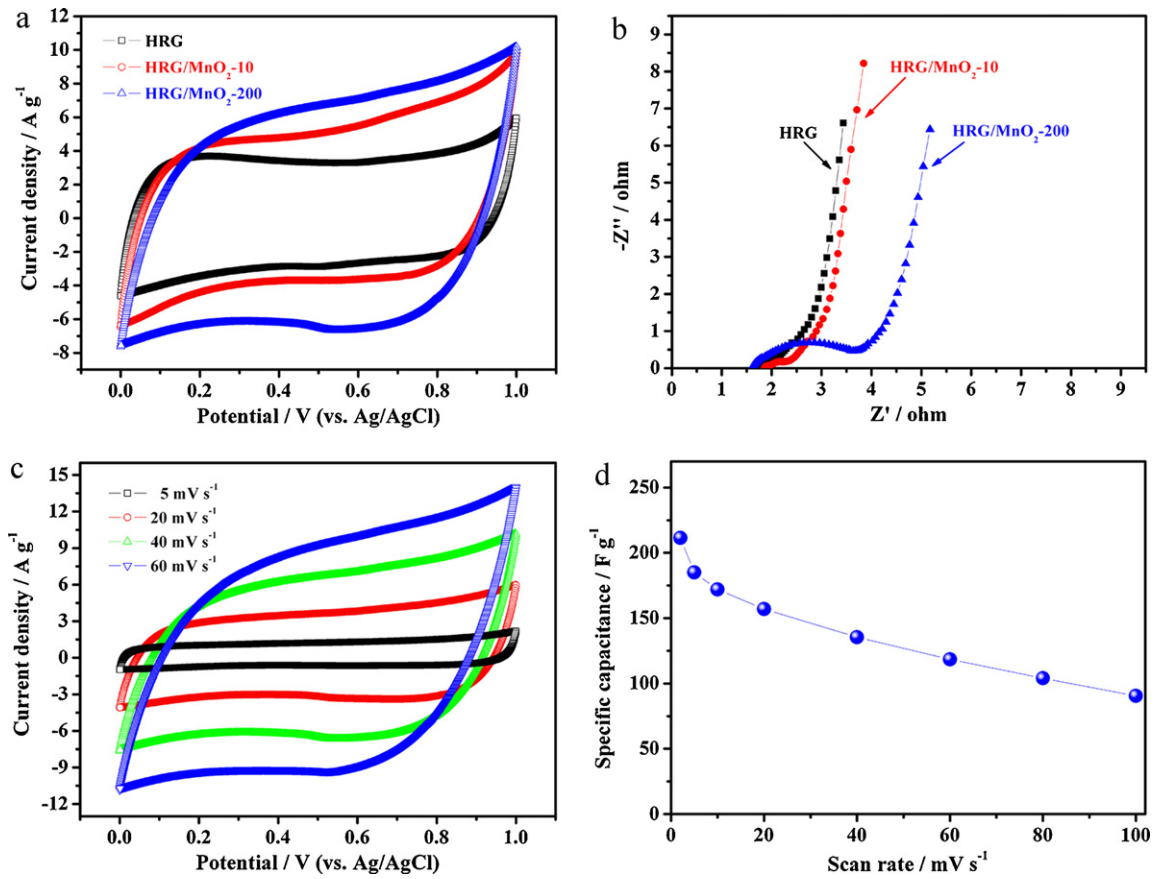

Fig. 5. (a) CV curves of HRG, HRG/MnO_2–10 and HRG/MnO_2–200 electrodes at a scan rate of 40 mV s^{-1} in 1 M Na_2SO_4 electrolyte; (b) Nyquist plots of HRG, HRG/MnO_2–10 and HRG/MnO_2–200 electrodes; (c) CV curves of HRG/MnO_2–200 electrode at different scan rates in 1 M Na_2SO_4 electrolyte; (d) the specific capacitance as a function of potential scan rates.

property and excellent reversibility of this electrode. The specific capacitance values as a function of potential scan rate is presented in Fig. 5d. The specific capacitance values calculated from different scan rates are 211.5, 185, 172, 157, 135.5, 118.5, 104 and 90.5 F g^{-1} at 2, 5, 10, 20, 40, 60, 80 and 100 mV s^{-1}, respectively, exhibiting the large specific capacitances and good power capability of the electrode.

The cycling stability of the HRG/MnO_2–200 electrode was also evaluated by CV test at a scan rate of 50 mV s^{-1} for 1000 cycles. As shown in Fig. 6, the capacitance of the electrode after 1000 cycle is smaller than that of the first cycle, which may be ascribed to the loose of the active materials in electrode and/or the mass losing of the electrode after 1000 times of cycle.

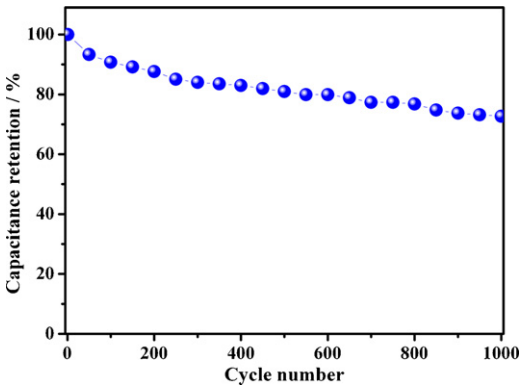

Fig. 6. Cycling stability of the HRG/MnO_2–200 electrode measured at 50 mV s^{-1}.

4. Conclusions

We have demonstrated a facile synthesis of HRG/MnO_2 composites by a room temperature redox deposition process, and investigated their electrochemical properties as supercapacitors. The opening porous morphology makes the electrolyte readily to get in touch with the surfaces of materials, which is important for generating high electrochemical performances. The specific capacitance values of HRG/MnO_2–200 electrode reached 211.5 F g^{-1} at a potential scan rate of 2 mV s^{-1} and with about 75% capacitance retention after 1000 times of charge/discharge cycle in 1 M Na_2SO_4 electrolyte, indicating a good application potential in supercapacitors as well as other power source systems.

Acknowledgements

We thank the National Natural Science Foundation of China (Grant Nos. 20823008 and 51075384) and "Top Hundred Talents Program" of Chinese Academy of Sciences for financial support.

Appendix A. Supplementary data

Supplementary data associated with this article can be found, in the online version, at doi:10.1016/j.jpowsour.2011.05.036.

References

[1] B.E. Conway, Electrochemical Supercapacitors, Scientific Fundamentals and Technological Applications, Kluwer Academic/Plenum Press, New York, 1999.
[2] L.L. Zhang, X.S. Zhao, Chem. Soc. Rev. 38 (2009) 2520.

[3] W. Xing, S.Z. Qiao, R.G. Ding, F. Li, G.Q. Lu, Z.F. Yan, H.M. Cheng, Carbon 44 (2006) 216.
[4] M. Winter, R.J. Brodd, Chem. Rev. 104 (2004) 4245.
[5] K.S. Novoselov, A.K. Geim, S.V. Morozov, D. Jiang, Y. Zhang, S.V. Dubonos, I.V. Grigorieva, A.A. Firsov, Science 306 (2004) 666.
[6] D. Chen, L. Tang, J. Li, Chem. Soc. Rev. 39 (2010) 3157.
[7] Z.S. Wu, W. Ren, L. Wen, L. Gao, J. Zhao, Z. Chen, G. Zhou, F. Li, H.M. Cheng, ACS Nano 4 (2010) 3187.
[8] B. Saner, F. Okyay, Y. Yürüm, Fuel 89 (2010) 1903.
[9] F. Schedin, A.K. Geim, S.V. Morozov, E.W. Hill, P. Blake, M.I. Katsnelson, K.S. Novoselov, Nat. Mater. 6 (2007) 652.
[10] L. Valentini, M. Cardinali, S.B. Bon, D. Bagnis, R. Verdejo, M.A. Lopez-Manchadob, J.M. Kenny, J. Mater. Chem. 20 (2010) 995.
[11] L.L. Zhang, R. Zhou, X.S. Zhao, J. Mater. Chem. 20 (2010) 5983.
[12] C.N.R. Rao, A.K. Sood, K.S. Subrahmanyam, A. Govindaraj, Angew. Chem. Int. Ed. 48 (2009) 7752.
[13] M.D. Stoller, S. Park, Y. Zhu, J. An, R.S. Ruoff, Nano Lett. 8 (2008) 3498.
[14] S.R.C. Vivekchand, C.S. Rout, K.S. Subrahmanyam, A. Govindaraj, C.N.R. Rao, J. Chem. Sci. 120 (2008) 9.
[15] Y. Wang, Z.Q. Shi, Y. Huang, Y.F. Ma, C.Y. Wang, M.M. Chen, Y.S. Chen, J. Phys. Chem. C 113 (2009) 13103.
[16] B.J. Lee, S.R. Sivakkumar, J.M. Ko, J.H. Kim, S.M. Jo, D.Y. Kim, J. Power Sources 168 (2007) 546.
[17] S.R. Sivakkumar, W.J. Kim, J.A. Choi, D.R. MacFarlane, M. Forsyth, D.W. Kim, J. Power Sources 171 (2007) 1062.
[18] F. Pico, J. Ibañez, M.A. Lillo-Rodenas, A. Linares-Solano, R.M. Rojas, J.M. Amarilla, J.M. Rojo, J. Power Sources 176 (2008) 417.
[19] D.W. Wang, F. Li, J. Zhao, W. Ren, Z.G. Chen, J. Tan, Z.S. Wu, I. Gentle, G.Q. Lu, H.M. Cheng, ACS Nano 3 (2009) 1745.
[20] H. Wang, Q. Hao, X. Yang, L. Lu, X. Wang, Electrochem. Commun. 11 (2009) 1158.
[21] P.J. Hung, K.H. Chang, Y.F. Lee, C.C. Hu, K.M. Lin, Electrochim. Acta 55 (2010) 6015.
[22] J. Xu, K. Wang, S.Z. Zu, B.H. Han, Z. Wei, ACS Nano 4 (2010) 5019.
[23] H. Wang, Q. Hao, X. Yang, L. Lu, X. Wang, ACS Appl. Mater. Interfaces 2 (2010) 821.
[24] H. Wang, Q. Hao, X. Yang, L. Lu, X. Wang, Nanoscale 2 (2010) 2164.
[25] Q. Wu, Y. Xu, Z. Yao, A. Liu, G. Shi, ACS Nano 4 (2010) 1963.
[26] J. Yan, T. Wei, Z. Fan, W. Qian, M. Zhang, X. Shen, F. Wei, J. Power Sources 195 (2010) 3041.
[27] J. Yan, T. Wei, B. Shao, Z. Fan, W. Qian, M. Zhang, F. Wei, Carbon 48 (2010) 487.
[28] X. Yan, J. Chen, J. Yang, Q. Xue, P. Miele, ACS Appl. Mater. Interfaces 2 (2010) 2521.
[29] K. Zhang, L.L. Zhang, X.S. Zhao, J. Wu, Chem. Mater. 22 (2010) 1392.
[30] A. Liu, C. Li, H. Bai, G. Shi, J. Phys. Chem. C 114 (2010) 22783.
[31] S. Biswas, L.T. Drzal, Chem. Mater. 22 (2010) 5667.
[32] L.L. Zhang, S. Zhao, X.N. Tian, X.S. Zhao, Langmuir 26 (2010) 17624.
[33] Z.S. Wu, D.W. Wang, W. Ren, J. Zhao, G. Zhou, F. Li, H.M. Cheng, Adv. Funct. Mater. 20 (2010) 3595.
[34] S. Chen, J. Zhu, X. Wu, Q. Han, X. Wang, ACS Nano 4 (2010) 2822.
[35] Z.S. Wu, W. Ren, D.W. Wang, F. Li, B. Liu, H.M. Cheng, ACS Nano 4 (2010) 5835.
[36] S. Chen, J. Zhu, X. Wang, ACS Nano 4 (2010) 6212.
[37] J. Yan, Z. Fan, T. Wei, W. Qian, M. Zhang, F. Wei, Carbon 48 (2010) 3825.
[38] F. Li, J. Song, H. Yang, S. Gan, Q. Zhang, D. Han, A. Ivaska, L. Niu, Nanotechnology 20 (2009) 455602.
[39] Y. Zhang, H. Li, L. Pan, T. Lu, Z. Sun, J. Electroanal. Chem. 634 (2009) 68.
[40] S. Chen, J. Zhu, X. Wang, J. Phys. Chem. C 114 (2010) 11829.
[41] H. Wang, H.S. Casalongue, Y. Liang, H. Dai, J. Am. Chem. Soc. 132 (2010) 7472.
[42] T. Lu, Y. Zhang, H. Li, L. Pan, Y. Li, Z. Sun, Electrochim. Acta 55 (2010) 4170.
[43] B. Wang, J. Park, C. Wang, G. Wang, Electrochim. Acta 55 (2010) 6812.
[44] J. Yan, T. Wei, W. Qiao, B. Shao, Q. Zhao, L. Zhang, Z. Fan, Electrochim. Acta 55 (2010) 6973.
[45] F.Y. Cheng, J. Chen, X.L. Gou, P.W. Shen, Adv. Mater. 17 (2005) 2753.
[46] W.S. Hummers, R.E. Offeman, J. Am. Chem. Soc. 80 (1958) 1339.
[47] S. Liu, J.Q. Wang, J. Zeng, J.F. Ou, Z.P. Li, X.H. Liu, S.R. Yang, J. Power Sources 195 (2010) 4628.
[48] Y. Xu, K. Sheng, C. Li, G. Shi, ACS Nano 4 (2010) 4324.
[49] X. Jin, W. Zhou, S. Zhang, G.Z. Chen, Small 3 (2007) 1513.
[50] S.W. Lee, J. Kim, S. Chen, P.T. Hammond, Y. Shao-Horn, ACS Nano 4 (2010) 3889.
[51] W. Xiao, H. Xia, J.Y.H. Fuh, L. Lu, J. Power Sources 193 (2009) 935.
[52] H.Q. Wang, G.F. Yang, Q.Y. Li, X.X. Zhong, F.P. Wang, Z.S. Li, Y.H. Li, New J. Chem. 35 (2011) 469.
[53] L. Tang, Y. Wang, Y. Li, H. Feng, J. Lu, J. Li, Adv. Funct. Mater. 17 (2009) 2782.
[54] A.V. Murugan, T. Muraliganth, A. Manthiram, Chem. Mater. 21 (2009) 5004.
[55] C. Julien, M. Massot, R. Baddour-Hadjean, S. Franger, S. Bach, J.P. Pereira-Ramos, Solid State Ionics 159 (2003) 345.
[56] S.B. Ma, K.Y. Ahn, E.S. Lee, K.H. Oh, K.B. Kim, Carbon 45 (2007) 375.
[57] J. Yan, Z.J. Fan, T. Wei, J. Cheng, B. Shao, K. Wang, L.P. Song, M.L. Zhang, J. Power Sources 194 (2009) 1202.
[58] M. Chigane, M. Ishikawa, J. Electrochem. Soc. 147 (2000) 2246.